Tightening Dynamics of Wound Rolls: The Interplay of Solid Friction and Interfacial Compressibility

M Caelen, Sebastien Moulinet, Bruno Andreotti, Frédéric Lechenault

Tightening Dynamics of Wound Rolls: The Interplay of Solid Friction and Interfacial Compressibility

M. Caelen, S. Moulinet, B. Andreotti, and F. Lechenault
Laboratoire de Physique de l'Ecole Normale Supérieure, PSL, Sorbonne Université, Université Paris Cité, CNRS, 24 rue Lhomond 75005 Paris, France.
(Dated: February 11, 2025)

The capstan equation predicts that the tension along a flexible band wrapped around a cylinder decreases exponentially with the number of turns due to solid friction. Consequently, it is expected that tightening a loosely prepared roll by pulling on the end of the band would be extremely difficult. However, we demonstrate in a controlled experiment that not only does the tightening of the loose winding occur, but it is actually induced and controlled by surface roughness, through solid friction and interfacial compressibility. The experiment reveals that a slipping zone nucleates on the fixed inner core and propagates outwards through a stick-slip sequence. As the slipping zone propagates outward, the gained slack accumulates, reducing the pressure exerted at the slipping point and facilitating the rewinding of the outer part of the roll onto its inner part.

Winding is a common industrial process used to convert thin sheet materials such as paper, metal foils, plastics, flexible packaging films, magnetic tape, cloth, or fabrics into compact rolls. This allows for convenient storing, handling, and transportation. Industrial rolls are typically wound by rotating a solid core while applying a controlled tension or normal stress to the elastic tape using a nip roller [1–3]. One of the primary challenges in the winding process is interlayer slippage, which can lead to internal buckling in wound rolls due to solid friction [4, 5]. To prevent this, a high interlayer pressure is required [6], particularly at high velocities where air can be trapped between roll layers due to viscous entrainment or mechanical vibrations [7, 8]. However, maintaining high normal stresses can also induce surface damage or even core collapse [9]. Applied mechanics studies have aimed to characterize the internal stress of rolls [10–15] and to develop homogenized models that do not resolve the thickness of the layers [16, 17]. However, the lap-by-lap construction of a wound roll stores the history of the loading in the material. The problem is further complicated by interfacial compressibility [18, 19] and the hysteretic nature of solid friction [20–22], both of which are caused by the tape's surface roughness.

When a roll is 'unwound', its central core is typically allowed to rotate freely. Here, we explore the opposite scenario where the core is held fixed, and the free outer end of the elastic tape is progressively pulled to eliminate residual slack (Fig. 1) and compact the roll. Following the capstan problem, one could postulate that if all layers were to slip over one another, the tension would decrease exponentially along the tape due to solid friction (see Supplemental Material [23]). This would result in localized stretching of the outermost layer, making it inefficient to tighten the roll's inner layers. By contrast, we demonstrate in this letter that tightening is achieved throughout the entire wound roll. This is accomplished through successive tightening waves, originating from the innermost layers and propagating outwards, that result

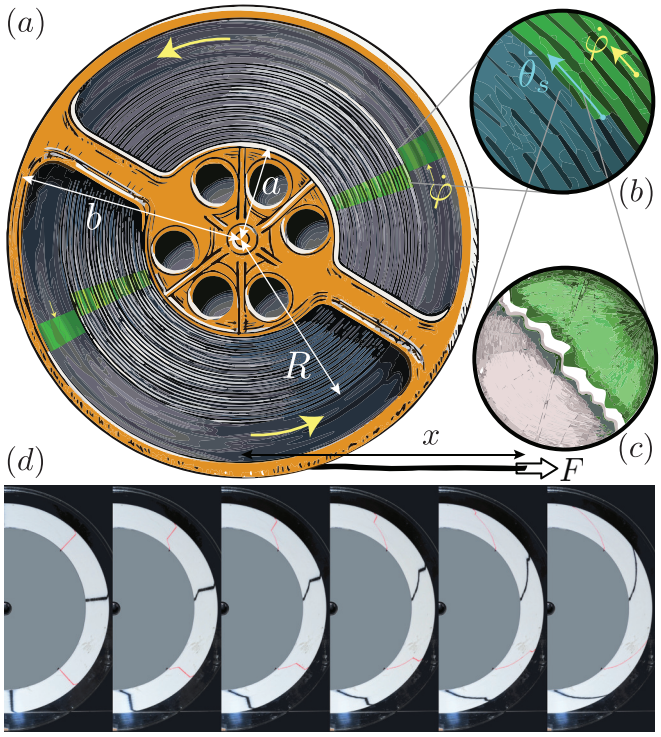

Figure 1. (a) Experimental set-up: a wound roll is fixed at one end to its static core while its other end is pulled with a force F. As a result, an outer region in solid body rotation is separated from a static inner region by a circular shear band, located at an increasing radius R. (b) Shear band: the inner roll (grey) is tighter than the outer roll (green) in solid rotation with angular velocity $\dot{\varphi}$. (c) Superficial roughness induces both solid friction and interfacial compressibility. (d) Series of images from an experiment. An initially straight pencil line is gradually sheared into an Archimedean spiral as one tightening wave propagates across the roll at a constant rate dR/dx.

in a sequence of minor decreases in interlayer spacing (Fig. 1). We show that this diminution in interlayer spacing leads to a gradual elimination of the residual slack by compressing the tape's interfacial roughness [18, 19]. A

key result of this study is the understanding of the origin of these waves and the determination of their propagation rate.

We conducted the experiment using various rolled materials, including plastic, curling ribbon, and fiberglass ribbon akin to that found in tailor's measuring tapes. We consistently observed the same phenomenology across these materials [23]. The quantitative analysis presented here was performed using a Super 8 leader tape, measuring 103.3 m in length and 8.0 mm in width, center-wound on a cylindrical core with a radius of 8.0 cm. Initially, one end of the tape is securely affixed to the core to prevent slippage. The winding process is initiated by rotating the core, with the entrained tape subjected to a regulated tension of ~ 1 N and a typical velocity of ~ 1 m/s. This is achieved by applying a constant frictional force to the free tape. Subsequently, the core is fastened to the base frame of an Instron force apparatus, inhibiting its rotation. The free outer end of the roll is then connected to the moving stage of the apparatus. In a standard experiment, the tape's extremity is pulled at a constant controlled velocity of $v = 0.1$ or 1 mm/s (with the extracted length denoted as $x = vt$) while the applied load F is recorded at an acquisition frequency of approximately 1 kHz. Imaging is conducted using a Nikon digital camera at 0.5 Hz, supplemented by a Phantom fast camera for short sequences at 1 kHz. In a typical run, we are able to extract more than 1 m of tape.

The Young's modulus of the tape in the elastic regime, equal to 2.7 GPa, is sufficiently high to prevent significant stretching under the experimental conditions employed. We therefore hypothesize that the roll can be approximated by an Archimedean spiral of an inextensible tape with a constant interlayer spacing equal to $h \equiv (b-a)/N$. Here, a and b represent the inner and outer radii of the roll (Fig. 1), respectively, and N is the fixed number of layers dictated by the roll's initial winding. Expressing the area $\pi(b^2 - a^2) = (L - x)h$, one finds that the outer radius b decreases linearly with the extracted length x, as described by the equation $\pi N\,(b(x) + a) = L - x$, where L is the roll's initial total length. Differentiating this equation yields:

$$\frac{\mathrm{d}b}{\mathrm{d}x} = -\frac{1}{\pi N}\ . \tag{1}$$

Experimentally, the outer radius b decreases in a stepwise manner but exhibits an overall linear decrease with the extracted length x (Fig. 2a). The slope $\mathrm{d}b\,/\,\mathrm{d}x$, measured for rolls with different lengths L and thus different numbers N of layers, adheres to the prediction of Eq. (1) (Fig. 2b). This sensitive test directly demonstrates that compaction results from a change in interlayer spacing with negligible change in length. Consequently, for a given change in the interlayer spacing h, the extractable length is proportional to N^2: there are N layers that become thinner, and each decrease in a layer's thickness affects the radii of all the layers above it.

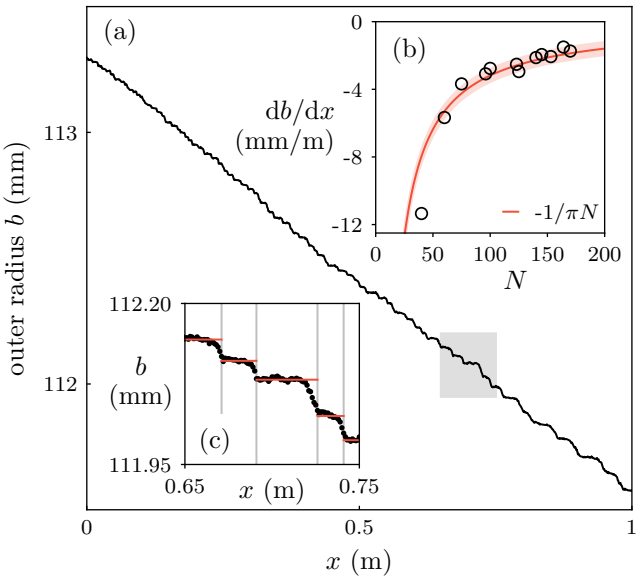

Figure 2. (a) Outer radius b as a function of the extracted length x, for a wound roll of 170 layers. (b) Mean slope $\mathrm{d}b\,/\,\mathrm{d}x$ as a function of the number of layers N. The exact prediction for an inextensible Archimedean spiral, as given by Eq. (1), is shown in red. The coloured region corresponds to a residual strain ϵ (see Eq. (5) in the SM [23]) with $d\epsilon/dx = \pm 0.2$ %/m. (c) Closeup of the grey square in (a). The grey vertical lines indicate drops in b separating plateaus (red).

The discontinuous evolution of the outer radius b on a small scale is associated with the propagation of a circular shear band from the inner static core to the roll's outer edge, as illustrated in Fig. 1 and [23]. This process can be interpreted as an intermittent rewinding of the roll, each time with a smaller interlayer spacing h. As the rotation proceeds, the outer region becomes thinner; when it vanishes, the roll's outer radius b suddenly drops by a finite amount δb (Fig. 2c), and a new tightening zone nucleates near the roll's inner radius (inset of Fig. 3). The location R of the shear band increases at a constant rate $\mathrm{d}R\,/\,\mathrm{d}x$ (Fig. 3) from its nucleation to its evacuation at the outer radius. This kinematics can be modeled by two spirals: an inner spiral and an outer spiral, connected at a polar coordinate (R, θ_s) that locates the position of the shear band. The connecting point follows a spiral with an interlayer spacing h, where an angular shift $\mathrm{d}\theta_s$ corresponds to a radial shift $\mathrm{d}R = \frac{h}{2\pi}\mathrm{d}\theta_s$. The outer spiral then undergoes solid rotation by an angle $\mathrm{d}\varphi = \mathrm{d}x/b$. The partial conversion of a tape element from a loose outer spiral at radius r_{out} to a tighter inner spiral at radius r_{in}, while the remainder continues in solid rotation, yields the relation $r_{\mathrm{out}}\mathrm{d}\theta_s = r_{\mathrm{in}}\mathrm{d}\theta_s + r_{\mathrm{out}}\mathrm{d}\varphi$. Combining these relations, we obtain a relationship between $\mathrm{d}R\,/\,\mathrm{d}x$, the rate of change of the radial position R of the shear band with respect to the extracted length x, and the ratio of R to the accumulated slack $\delta R = r_{\mathrm{out}}(\theta_s) - r_{\mathrm{in}}(\theta_s)$

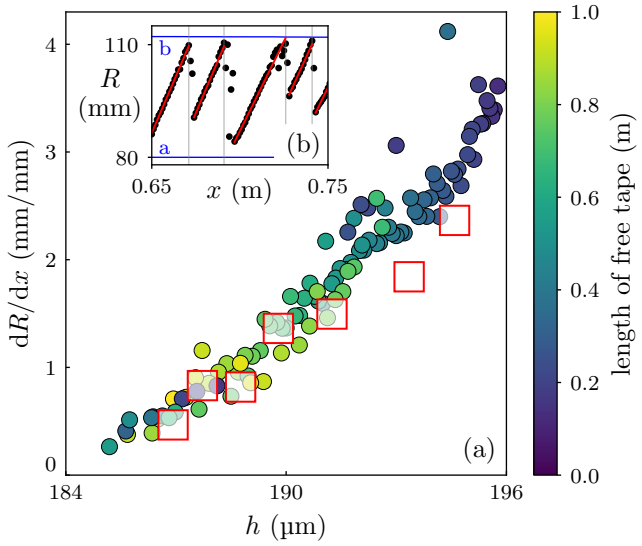

Figure 3. (a) Propagation rate $\mathrm{d}R\,/\,\mathrm{d}x$ of the shear band as a function of the interlayer spacing $h \equiv (b-a)/N$. The circles represent the slopes $\mathrm{d}R\,/\,\mathrm{d}x$ from Fig. 2b and other experiments, with their color indicating the length of free tape. The red squares correspond to the kinematic prediction from Eq. (2), using the value of δR measured from the discontinuous drops of b in Fig. 2a. (b) Radial location R of the shear band as a function of x for the same experiment as in Fig. 2c. The grey vertical lines indicate the points at which the shear band reaches the roll's outer radius b (red line) as in Fig. 2c

.

at the shear band:

$$\frac{\mathrm{d}R}{\mathrm{d}x} = \frac{h}{2\pi b}\frac{R}{\delta R}\ . \tag{2}$$

Measuring the outer radius b of the roll on images allows us to deduce the interlayer spacing h independently of the propagation rate $\mathrm{d}R\,/\,\mathrm{d}x$. Figure 3 presents the measurements obtained for various initial lengths of free tape and different extracted lengths during traction. The data points fall on a master curve providing further proof that the elasticity of the free length of the tape is not relevant in the tightening process. By employing Eq. (2), where the drops in outer radius δb provide an estimation of δR, we obtain consistent results.

The inset of Fig. 4 shows the pulling force F recorded during the process for rolls with different numbers N of layers. Despite a jagged appearance, the curves show an exponential increase of F with the extracted length x, with a rate that depends on N. As the increase in force is correlated with a decrease in the external radius, and knowing that the tape is not significantly stretched during the tightening process, we can infer that the strengthening of the system results from the lateral compression of the tape. We used the force apparatus to compress a stack of N 10 cm long strips of tape, with N ranging from 10 to 50. This calibration test, depicted by the diamonds in Fig. 4, shows that the interlayer distance h between

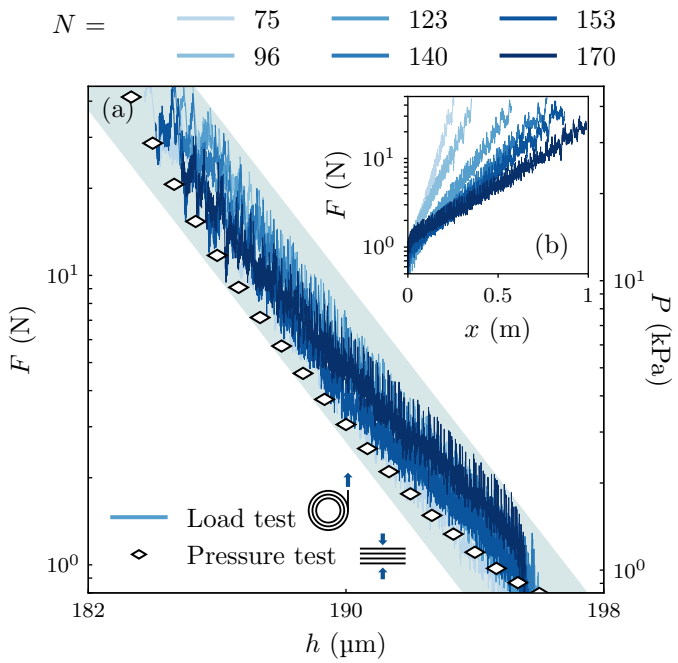

Figure 4. (a) The lines represent the load F as a function of the layer thickness h for wound rolls of different numbers of layers N. The blue zone represents the systematic uncertainty on h in our image analysis: while the relative uncertainty is very small, the absolute position of the curves on the horizontal axis is within 1%. The diamonds represent the pressure P needed to compress piles of strips of tape [23]. The correspondance of the left and right vertical axes is based on Eq. (3), taking $b = 10.4\,\mathrm{cm}$ as the mean outer radius over all the experiments. (b) Load F as a function of the extracted length x.

each strip depends logarithmically on the pressure P: $h = h_0\ \ln(P/P_0)$. This is the characteristic signature of the compression of interfacial roughness, which is also responsible for solid friction [24]. This explains how the inextensible strip can be tightened even though the bulk of the material is incompressible. Examination of our plastic samples' surfaces using AFM reveals a multi-scale roughness typical of plastic surfaces [18, 19], explaining this superficial compressibility [23].

The force peaks in Fig. 4 occur during a drop in R, which corresponds to the formation of a new tightening wave near the central core at $R \approx a$. The nucleation of a shear band occurs when the external torque bF balances the moment of frictional forces, yielding:

$$F = 2\pi\mu w\frac{a^2}{b}P\ . \tag{3}$$

Since there is no accumulated slack in the shear band, when it reforms, the pressure P can be estimated as that associated with the thickness $h \equiv (b-a)/N$. Here, $\mu \simeq 0.31$ represents the static friction coefficient, calibrated independently [23]. Recent studies have revisited the initiation of sliding, proposing a nucleation phase

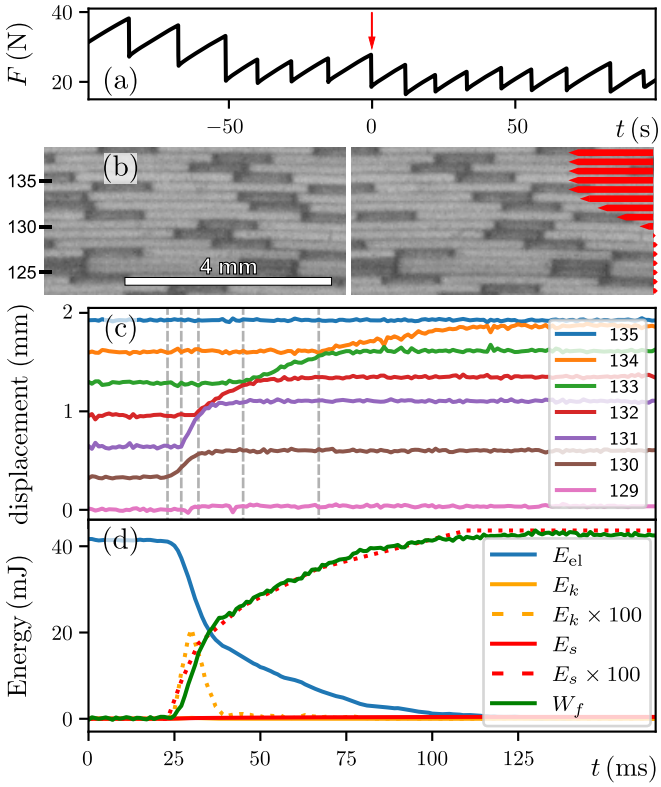

Figure 5. (a) Force signal showing stick-slip behavior. The red arrow points to the slip event studied in the rest of the figure. (b) Closeup of the spool before (right) and after (left) the slip event. The two images are separated by 90 ms. The scale on the left indexes the layers, from the inside to the outside. The red arrows depict the shift of each layer during the slip event. A small retrograde motion is detected for the interior layers. (c) Relative displacement of the layers involved in the slip event with respect to their inward neighbor. For clarity, the curves are shifted vertically. The vertical dashed lines indicate the times at which the layers, numbered 130 to 134, start to slip. (d) Comparison between the evolution of different types of energy during the event. As E_k and E_s are much smaller than the other types of energy, their values multiplied by 100 are shown in dotted lines.

akin to a depinning transition, followed by a propagation phase [21, 22, 25, 26]. Toy models exploring the complex intermittent dynamics of frictional slips reveal significant spatio-temporal complexity [25, 27]. In such scenarios, μ would more closely resemble a dynamic friction coefficient. This equation predicts that the pulling load F is proportional to P and therefore decreases exponentially with the interlayer spacing h. Figure 4 shows that this relation is verified, without any adjustable parameters, for rolls consisting of different numbers of layers.

The intermittent curve of the load F versus x displays a succession of linear increases followed by abrupt drops (Fig. 5a), indicative of typical stick-slip motion. Slip events (drops of F) correspond to the circular shear band propagating by 3 to 5 layers (Fig. 5b and [23]). Recording such an event with the fast camera allowed us to track the shear displacement of each layer relative to its predecessor. When one layer starts to slip on its inward neighbor, the latter has almost stopped its own motion (Fig. 5c). This shows that at any time, the friction between layers is localized on the roll in a region of the order of only one turn. We estimated the elastic energy E_{el} released during the slip phase by modeling the system as a spring during the load in the stick phase, when the force linearly increases prior the slip event. This energy can be converted into three forms: kinetic energy E_k, energy stored in the radial compression of the band E_s, or dissipated by solid friction. Measuring the velocity and the length of the moving part with the fast camera leads to the estimate of E_k. E_s is assimilated to the work of the pressure P, deduced from the Eq. (3), over a variation of h deduced from δb. The same expression of P is used to determine the work of solid friction W_f along the distance covered by the shear band. Although most of the energy is dissipated through solid friction, a small fraction, typically around 1%, is transferred to kinetic energy before being utilized to retighten the band (Fig. 5d).

In conclusion, the tightening of a wound roll is governed by two distinct properties induced by the surface roughness of the films: solid friction and interfacial compressibility. Unlike systems where the coupling between solid friction and elasticity results in a scale-free distribution of plastic events reminiscent of seismicity [28–30], the tightening process described here propagates successive rewinding fronts across the entire system in a nearly deterministic manner. The stick-slip dynamics are influenced by the exponentially increasing pressure within the system, nucleating increasingly large and rare tightening steps. Meanwhile, the propagation of the shear band is stabilized by the local loosening of the roll, associated with the continuous emission of slack from the rewinding dynamics. In this sense, the observed dynamics bear similarities to the ruck in a rug problem [31, 32], with one significant difference: solid friction is never eliminated, as the void space is located between the surface roughness of the material.

[1] A. Penner, Tappi journal **74**, 160 (1991).
[2] J. K. Good, Z. Wu, and M. W. R. Fikes, Journal of Applied Mechanics-Transactions of the ASME **61**, 182 (1994).
[3] M. Jorkama and R. von Hertzen, Journal of Pulp and Paper Science **28**, 280 (2002), 86th Annual Meeting of the Pulp-and-Paper-Technical-Association-of-Canada, Montreal, Canada, Jan 31-Feb 04, 2000.
[4] P. M. Lin and J. A. Wickert, Journal of Manufacturing Science and Engineering-Transactions of the ASME **128**, 56 (2006).
[5] C. Lee, International Journal of Precision Engineering and Manufacturing **19**, 781 (2018).
[6] N. Vaidyanathan, A study on wound roll slippage (Oklahoma State University, 1996).

[7] K. L. Knox and T. L. Sweeney, Industrial & Engineering Chemistry Process Design and Development **10**, 201 (1971).
[8] J. Good and M. Holmberg, Proceedings of the International Conference on Web Handling , 246 (Oklahoma State University, 1993).
[9] H. Yagoda, Journal of Applied Mechanics **47**, 847 (1980).
[10] J. Pfeiffer, Tappi Journal **49**, 342 (1966).
[11] H. Altmann, Tappi Journal **51**, 176 (1968).
[12] H. Yagoda, Mechanics Research Communications **7**, 103 (1980).
[13] Z. Hakiel, Tappi Journal **70**, 113 (1987).
[14] M. Willett and W. Poesch, Journal of Applied Mechanics **55**, 365 (1988).
[15] R. Benson, Journal of Applied Mechanics **62**, 853 (1995).
[16] N. Zabaras and S. Liu, Acta Mechanica **111**, 95 (1995).
[17] G. Zurlo and L. Truskinovsky, Physical Review Letters **119**, 048001 (2017).
[18] M. Benz, K. J. Rosenberg, E. J. Kramer, and J. N. Israelachvili, The Journal of Physical Chemistry B **110**, 11884 (2006).
[19] B. Persson, Physical review letters **99**, 125502 (2007).
[20] T. Baumberger and C. Caroli, Advances in Physics **55**, 279 (2006).
[21] S. Gvirtzman and J. Fineberg, Journal of Geophysical Research: Solid Earth **128**, e2022JB025483 (2023).
[22] S. Gvirtzman, D. S. Kammer, M. Adda-Bedia, and J. Fineberg, Nature **637**, 369 (2025).
[23] See Supplemental Material at URL-will-be-inserted-by-publisher for further details.
[24] B. N. Persson, Surface science reports **61**, 201 (2006).
[25] T. Strunz and F.-J. Elmer, Physical Review E **58**, 1612 (1998).
[26] V. Dawara and K. Viswanathan, Physical Review E **110**, 025004 (2024).
[27] A. Vanossi, N. Manini, F. Caruso, G. E. Santoro, and E. Tosatti, Physical review letters **99**, 206101 (2007).
[28] J. L. Barrat, The European Physical Journal E **20**, 355 (2006).
[29] R. Baggio, O. Salman, and L. Truskinovsky, Physical Review E **107**, 025004 (2023).
[30] A. Nicolas, E. E. Ferrero, K. Martens, and J.-L. Barrat, Reviews of Modern Physics **90**, 045006 (2018).
[31] J. M. Kolinski, P. Aussillous, and L. Mahadevan, Physical review letters **103**, 174302 (2009).
[32] D. Vella, A. Boudaoud, and M. Adda-Bedia, Physical review letters **103**, 174301 (2009).